First-principles theory of ultrathin magnetic films

1999 J. Phys.: Condens. Matter 11 9347

(http://iopscience.iop.org/0953-8984/11/48/302)

J. Phys.: Condens. Matter **11** (1999) 9347–9363. Printed in the UK PII: S0953-8984(99)08324-1

First-principles theory of ultrathin magnetic films

T Asada†, G Bihlmayer‡, S Handschuh‡, S Heinze‡§, Ph Kurz‡ and S Blügel‡

† Faculty of Engineering, Shizuoka University, Hamamatsu 432, Japan
‡ Institut für Festkörperforschung, Forschungszentrum Jülich, D-52425 Jülich, Germany
§ Zentrum für Mikrostrukturforschung, Universität Hamburg, D-20355 Hamburg, Germany

E-mail: s.bluegel@fz-juelich.de

Received 30 September 1999

Abstract. We report on a set of systematic first-principles electronic structure investigations of the magnetic spin moments, the magnetic spin configurations, and the magnetic coupling of ultrathin magnetic films on (001)- and (111)-oriented noble-metal substrates and on the Fe(001) substrate. Magnetism is found for 3d-, 4d-, and 5d-transition-metal monolayers on noble-metal substrates. For V, Cr, and Mn on (001) substrates a c(2×2) antiferromagnetic superstructure has the lowest energy, and Fe, Co, Ni are ferromagnetic. On (111) substrates, for Cr the energy minimum is found for a 120° non-collinear magnetic configuration in a $(\sqrt{3} \times \sqrt{3})$R30° unit cell, and for Mn a row-wise antiferromagnetic structure is found. On Fe(001), V and Cr monolayers prefer the layered antiferromagnetic coupling, and Fe, Co, and Ni monolayers favour the ferromagnetic coupling to Fe(001). The magnetic structure of Mn on Fe(001) is a difficult case: at least two competing magnetic states are found within an energy of 7 meV. The Cr/Fe(001) system is discussed in more detail as the surface-alloy formation is investigated, and this system is used as a test case to compare theoretical and experimental scanning tunnelling spectroscopy (STS) results. The possibility of resolving magnetic structures by STS is explored. The results are based on the local spin-density approximation and the generalized gradient approximation to the density functional theory. The calculations are carried out with the full-potential linearized augmented-plane-wave method in film geometry.

1. Introduction

Scientific and technical advances have created unprecedented new opportunities for designing artificial materials. Among them are epitaxially grown magnetic ultrathin 3d-transition-metal films stabilized on various non-magnetic and magnetic substrates (for reviews see references [1, 2]).

For instance, magnetic films grown on noble-metal substrates are examples of two-dimensional (2D) systems, and the electronic structure, the magnetic moments, the magnetic structure, the structural properties, the magneto-crystalline anisotropy, the critical properties, and the magnetic phase transition are significantly different from those of bulk systems. The focus of the investigation has centred on the itinerant magnetism of 3d-metal films. The search for new ultrathin magnetic material with possibly new magnetic properties had been extended to 4d [3–6] and 5d [7] transition metals on noble metals which has stimulated the search for magnetism in clusters in the gas phase [8, 9]. Additional complexity is added by growing material in new atomic ground-state structures, i.e. c(2×2) Mn [10], fcc Fe [11], and bcc [12] and fcc [13] Co on suitable substrates, or modifying the electronic structure with adsorbates [14].

0953-8984/99/489347+17$30.00

It is fair to state that most *ab initio* calculations are centred around 3d-metal monolayers on (001)-oriented noble-metal substrates as discussed in several review articles [15, 16]. These systems can be considered as experimental realizations of two-dimensional magnets with little influence on the magnetic properties from the substrate. For these monolayer systems it was found (i) that the magnetic moments of the ultrathin films are very large, approaching the atomic limit, and (ii) that there are two competing magnetic phases: a p(1×1) ferromagnetic phase (all moments within the monolayer are aligned parallel) and an in-plane c(2×2) antiferromagnetic phase (a checkerboard-type arrangement of up and down moments at nearest-neighbour sites). A general trend was discovered: early transition metals (V, Cr, and Mn) prefer the antiferromagnetic superstructure and late transition metals (Fe, Co, and Ni) are stable in the ferromagnetic state. The magnetism is controlled by the hybridization between d electrons on nearest-neighbour (n.n.) sites (n.n. in-plane d–d hybridization), denoted in terms of a simplified spin model by an in-plane exchange coupling $J_{\parallel}$.

Antiferromagnetic interactions on a triangular lattice are the origin of frustrated spin systems. A triangular lattice is readily provided by (111)-oriented noble-metal substrates or by pseudo-hexagonal growth—for example of c(8×2)Mn on Cu(100) [17]. Assuming for the magnetic description of these monolayer systems on a triangular lattice a classical nearest-neighbour Heisenberg model with antiferromagnetic interactions, a non-collinear spin structure is expected as the ground state with magnetic moments of each atom aligned at $\pm 120^{\circ}$ compared to the moments of the neighbouring atoms: the $(\sqrt{3} \times \sqrt{3})$R30° non-collinear spin structure with three atoms per surface unit cell. Experimentally as well as theoretically, these non-collinear structures are largely unexplored.

Gunnarsson [18] and Janak [19] investigated the possibility of spontaneous magnetizations for 4d bulk metals. They found that with intra-atomic exchange integrals, $I_{4\mathrm{d}}$, of about 0.65 eV and local densities of states (LDOS), n_{loc}, at the Fermi energy (ϵ_F) varying from 0.32 states eV^{-1}/spin for Mo to 1.15 states eV^{-1}/spin for Pd, the Stoner criterion $n_{loc}(\epsilon_F)I > 1$ is never satisfied for any 4d metal. Following the general trend of decreasing localization of valence d wavefunctions when moving from the 3d to the 4d and 5d series, we find consequently an increase of the d bandwidth and a reduction of the LDOS, $n_{3\mathrm{d}} > n_{4\mathrm{d}} > n_{5\mathrm{d}}$, at the Fermi energy. In view of this and the fact that the exchange integral also decreases as $I_{3\mathrm{d}} > I_{4\mathrm{d}} > I_{5\mathrm{d}}$, bulk 5d magnetism becomes extremely unlikely and was never considered. On the other hand due to the reduction of the coordination number of transition-metal atoms in a monolayer film the bandwidth decreases and the LDOS at ϵ_F increases. Indeed magnetism with fairly large magnetic moments was found e.g. for Ru and Rh on Ag and Au [4, 5].

A second important issue in this field is the coupling of different magnetic materials across a common interface. The investigation of magnetic properties at such interfaces is intimately related to the phenomena of interlayer exchange coupling [20, 21], the giant magneto-resistance [22, 23], and the spin-valve realization [24] for which for example Cr/Fe(001) [25, 26] and Mn/Fe(001) [24], respectively, developed to model systems. At present, the magnetic properties of such interfaces, largely prepared by the deposition of ultrathin magnetic films on Fe(001) substrate, are under intensive experimental investigation: V/Fe(001) [27], Cr/Fe(001) [28], Mn/Fe(001) [29], Co/Fe(001) [30], Ni/Fe(001) [31]. The outcome on the magnetic coupling is partly contradictory, particularly at the monolayer range of coverage. At the monolayer range, different growth conditions such as layer-by-layer growth, island growth, and interface alloy formation may occur within small temperature ranges. Due to the sensitive interrelation of magnetism and the atomic structure of these systems, we expect that any change of the structure or morphology will result in changes of the magnetism. As we will see below, this is especially critical for Cr and Mn films. Particularly for Mn on Fe(001), there is a significant lack of microscopic experimental information on the surface

morphology after growth.

There have been far fewer theoretical investigations of 3d-metal monolayers on magnetic transition-metal substrates than on noble-metal substrates. The relative neglect is certainly due to complications related to the additional degrees of freedom for the magnetic coupling caused by the additional d–d hybridization across the interface. Since the d electrons of such magnetic substrates play an active role in determining the magnetic properties, one basically deals with three different exchange-coupling parameters J, which determine the magnetic coupling at the interface: (i) the exchange-coupling parameter $J_{\parallel}$ within the monolayer plane; (ii) the parameter $J_{\perp}$ of exchange coupling between the monolayer and the substrate, and (iii) the exchange-coupling parameter of the (bulk) substrate J_b. Thus 3d monolayers on magnetic transition-metal substrates are semi-infinite magnetic systems as opposed to the two-dimensional magnetic monolayers on noble-metal substrates, but in contrast to the case for plain transition-metal surfaces the coupling of the monolayer to the substrate ($J_{\perp}$) and the exchange coupling within the monolayer ($J_{\parallel}$) are substantially altered. Depending on the signs and relative strength of $J_{\parallel}$ and $J_{\perp}$, several different spin configurations can be anticipated (cf. figure 1): (i) a ferromagnetic monolayer coupling ferromagnetically to the substrate (p(1 $\times$ 1) ferromagnetic order); or (ii) a ferromagnetic monolayer coupling antiferromagnetically to the substrate (p(1 $\times$ 1) layered antiferromagnetic order); or (iii) an intrinsically c(2 $\times$ 2) antiferromagnetic monolayer, which has though to compromise with the existing ferromagnetic phase of the Fe(001) substrate, coupling c(2 $\times$ 2) (anti)ferrimagnetically. Finally, total-energy calculations are required to determine the minimum-energy magnetic state among the various metastable solutions. This, together with the additional complication that the interface relaxation which is largely determined by the d–d hybridization may interrelate with the minimum-energy magnetic state, has delayed *ab initio* calculations for these systems.

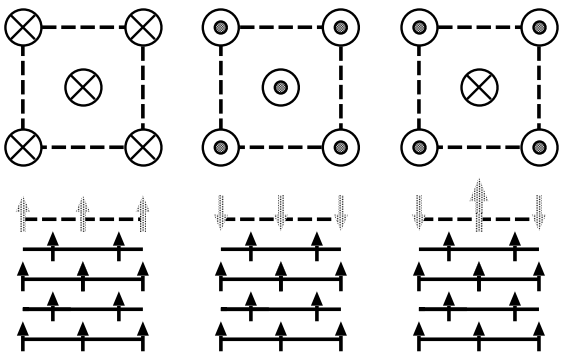

Figure 1. A schematic representation of a ferromagnetic, a layered antiferromagnetic, and a c(2 $\times$ 2) (anti)ferrimagnetic superstructure of a monolayer film (broken line) grown as an overlayer on a magnetic substrate (full line). In each case, the upper panel is a view onto the surface; the lower panel shows a side view. Arrows indicate the relative spin directions at the positions of the atoms.

In this paper we first briefly review the present understanding of 3d-, 4d-, and 5d-transition-metal monolayers on (001)-oriented fcc substrates. Then we investigate the ground-state spin structure of Cr and Mn monolayers beyond the Heisenberg model by performing *ab initio* calculations based on the vector spin-density functional theory. We discuss (111) unsupported (free-standing) monolayers (UML) of Cr and Mn with the lattice constant of Cu as a good

approximation to the overlayers on true Cu(111) and Ag(111) substrates. Then, we report on a set of systematic investigations of 3d-transition-metal (V, Cr, Mn, Fe, Co, Ni) monolayers as overlayers on Fe(001). Our attention will be focused on the stability of the three different competing phases: the p(1×1) ferromagnetic, the p(1×1) layered antiferromagnetic, and the c(2×2) ferrimagnetic spin configurations. For Mn monolayers on Fe(001), additional spin configurations are included in the search for the low-energy spin structure. Finally we discuss the system Cr/Fe(001) in more detail. We estimate on the basis of total-energy arguments the possibility for alloy formation between Cr and Fe at the Fe(001) surface. We make calculations for scanning tunnelling spectroscopy (STS) of the surface alloy and compare the results to experimental data. We explore the possibility of identifying different magnetic structures of a Cr monolayer by STS as well as that of distinguishing the chemical character of a Cr monolayer with different spin structures from the clean Fe(001) surface. The identification on the atomic scale of chemical species of a multi-component surface as it arises in the formation of surface alloys, in conjunction with the identification of their magnetic alignment and magnetic structure, is a key issue in the context of nano-magnetism. It is a problem ideally suited to investigation by a real-space probe such as scanning tunnelling microscopy, preferably with spin selectivity.

2. Method

The results are obtained in the context of the density functional theory. The calculations are carried out with the full-potential linearized augmented-plane-wave (FLAPW) method in film geometry [32] as implemented in the computer code FLEUR. Total-energy calculations are performed to search for the magnetic ground-state structure; force calculations are used for dynamical structure optimization. Spin–orbit interaction is included to determine the magneto-crystalline anisotropy energy. The results on the noble-metal substrates and the discussion of the system Cr/Fe(001) rely on the local spin-density approximation (LSDA) of von Barth and Hedin [33], but with parameters as chosen by Moruzzi, Janak, and Williams [34], and the results on the Fe substrate are obtained with the generalized gradient approximation (GGA) [35] and the theoretically determined GGA lattice constant of Fe, $a_0 = 5.33$ au, which is smaller by 1.5% than the experimental value of 5.41 au. Recently, the method has been extended to describe the inter-atomic non-collinear magnetism of 3d metals, in an environment with low symmetry and open structures [36].

3. Results

3.1. Monolayers on noble-metal substrates

3.1.1. Ferromagnetic monolayers on (001)-oriented noble-metal substrates. The intensive calculations (cf. figure 2(a)) for 3d-metal monolayers on the Ag(001) [37] substrate reveal that

(i) all 3d-metal monolayers (Ti, V, Cr, Mn, Fe, Co, Ni) show ferromagnetic solutions;
(ii) among the 3d metals the largest local moment of about 4 μ_B is found for Mn;
(iii) from Mn to Ni the magnetic moment decreases in steps of 1 μ_B (points (ii) and (iii) are reminiscent of Hund's first rule or the dominance of intra-atomic exchange);
(iv) the magnetic moments of Ti, V, and Cr monolayers show a pronounced dependence on the substrate: Ti is magnetic on Ag, but non-magnetic on Pd [38]; the magnetic moment of V is reduced by more than 1.5 μ_B when changing the substrate from Ag to Pd; and for Cr the magnetic moment changes from 3.8 μ_B as an adlayer on Ag or Pd to zero as an adlayer on Cu. Although not as dramatic, the reduction is also visible for Mn. We attribute the

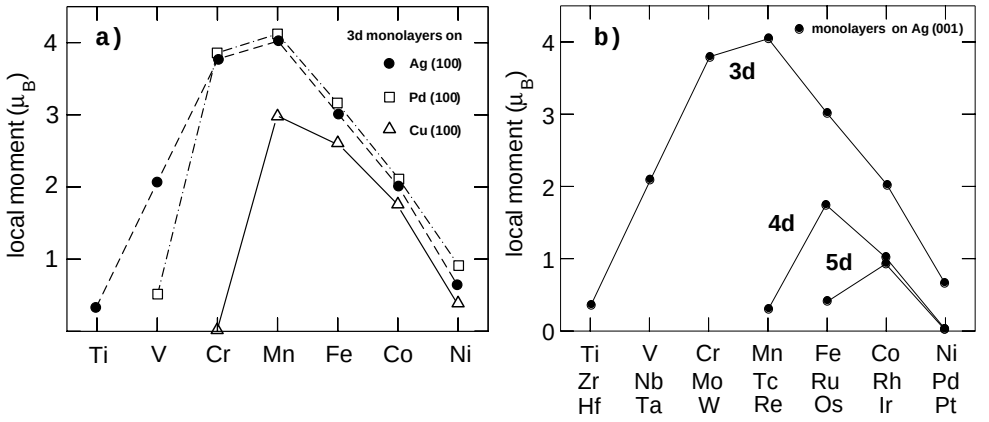

Figure 2. Local magnetic moments as calculated for ferromagnetic (a) 3d monolayers as overlayers on Ag(001) [37] (solid circles connected by a dashed line), Pd(001) [38] (empty squares connected by a chain line), and Cu(001) [40] (empty triangles connected by a solid line), and (b) 3d, 4d [5], and 5d [7] monolayers on Ag(001).

drastic reductions of the monolayer moments to the reduction of lattice constants in the sequence Ag to Pd to Cu.

On the other hand some of the local magnetic moments for the 3d monolayers are very large, and surprisingly magnetism with large magnetic moments was found for several of the 4d [5] and 5d [7] ones (cf. figure 2(b)): among the 4d metals, Tc, Ru, and Rh are ferromagnetic on Ag like Ru and Rh on Au; and among the 5d metals, Os and Ir are magnetic on Ag, but only Ir is magnetic on Au. No monolayer magnetism was found for 4d metals on Pd with the exception of Ru for which a rather small magnetic moment of 0.2 μ_B was calculated. Therefore, no 5d-monolayer magnetism on Pd is expected. When comparing the results for the local moments between 3d, 4d, and 5d monolayers on Ag(001) or Au(001) a remarkable trend is observed: the element with the largest magnetic moment among each transition-metal series is shifted from Mn to Ru (isoelectronic to Fe) and finally to Ir (isoelectronic to Co), respectively. Following these trends, we do not expect ferromagnetism for any other 4d or 5d metal on noble-metal (001) substrates, and indeed Mo and Re remained non-magnetic. The overall picture of monolayers on Ag and Au is the same, but the different substrate interactions cause Tc and Os on Au to be non-magnetic and lead to a slightly larger moment for Rh. Pd and Pt are predicted to be non-magnetic. Thus with Ti, V; Tc, Ru, Rh; Os, and Ir on Ag or Au, we found transition metals which are magnetic in 2D and non-magnetic in three dimensions. Recent investigations [39] including the spin–orbit interaction have shown that the spin–orbit interactions reduce significantly the magnetic spin moment of the 5d-metal monolayers and the spin moment might be suppressed.

3.1.2. Antiferromagnetic monolayers on (001)-oriented noble-metal substrates. It is by no means clear whether the ferromagnetic state is actually the magnetic ground state. In reality, various antiferromagnetic states as well as non-collinear spin configurations could be anticipated. The situation becomes relatively simple if we recall that the hybridization between the d electrons on nearest-neighbour sites is the dominating one. Therefore, one expects that the magnetic interaction should be described by a nearest-neighbour Heisenberg model. Then, for the square lattice as formed by the (001) monolayers, there are only two phases to be

considered: the ferromagnetic p(1×1) structure discussed in the previous section and the antiferromagnetic c(2×2) superstructure (a checkerboard arrangement of up and down spins similar to the c(2×2) ferrimagnetic structure in figure 1, but with identical magnetic moments on two magnetically inequivalent lattice sites).

Figure 3 shows the local moments for the antiferromagnetic c(2×2) phase of 3d monolayers on Ag(001) [37] together with the ferromagnetic moments. It becomes evident that, in general, antiferromagnetic and ferromagnetic moments have nearly the same values. This shows that in almost all cases both configurations exist and are of comparable energetic stability. No antiferromagnetic solutions exist at the beginning and at the end of the 3d series on Ag(001). A reliable total-energy calculation was performed in order to decide which configuration is the magnetic ground state and which one is a metastable one. Figure 3 shows the energy differences $\Delta E = E_{AFM} - E_{FM}$ per atom between the antiferromagnetic and the ferromagnetic configurations for 3d monolayers on Cu(001) [40] and Ag(001) [37]. A clear trend emerges: the Ni, Co, and Fe overlayers ($\Delta E > 0$) prefer the ferromagnetic configuration and the Mn, Cr, and V ones favour the antiferromagnetic one. From the strong similarities of the monolayer trends for these two substrates, we conclude that this is a general trend: Fe, Co, and Ni favour the p(1×1) ferromagnetism on the (001) surfaces of Pd, Pt and the noble metals Cu, Ag, and Au [41], whereas V, Cr, and Mn monolayers prefer the c(2×2) antiferromagnetic configuration. The same trend is expected for Al substrates although V and Ni might be non-magnetic.

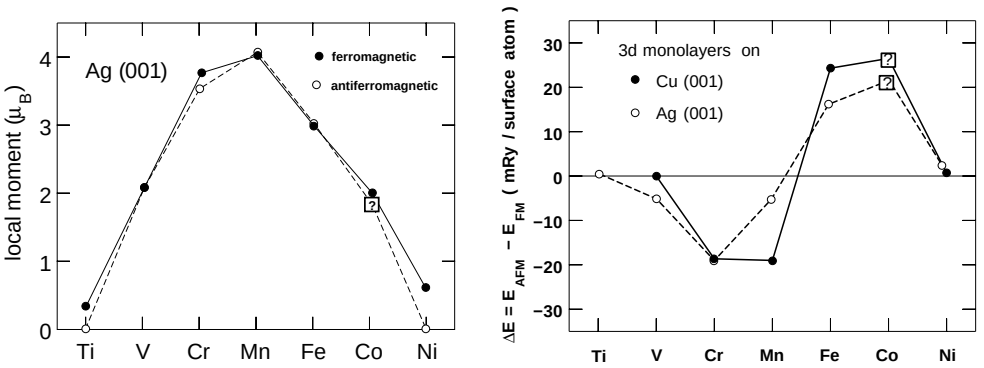

Figure 3. Left panel: local magnetic moments of 3d monolayers on Ag(001) [37] calculated for the p(1×1) ferromagnetic (solid circles connected by a full line) and the c(2×2) antiferromagnetic configuration (open circles connected by a dashed line). Right panel: total-energy difference $\Delta E = E_{AFM} - E_{FM}$ per 3d atom between the p(1×1) ferromagnetic and c(2×2) antiferromagnetic phase for 3d monolayers on Ag(001) [37] (open circles connected by a dashed line), and on Cu(001) [40] (solid circles connected by a full line). $\Delta E > 0$ (<0) means that the ferromagnetic (antiferromagnetic) configuration is the most stable one. '?' indicates a result which is not fully converged.

3.1.3. Magnetism of Cr and Mn monolayers on the triangular lattice. From the discussion above it is clear that Cr and Mn monolayers are two-dimensional antiferromagnets on the square lattice of the (001)-oriented noble-metal substrate. This suggests an antiferromagnetic n.n. coupling constant $J_{\|}$ in the classical Heisenberg model. Applied to Cr and Mn monolayers on the triangular lattice, it suggests the existence of a non-collinear spin structure as ground state in a $(\sqrt{3} \times \sqrt{3})$R30° unit cell containing three atoms with magnetic moments of each atom aligned at $\pm 120°$ compared to the moments of the neighbouring atoms.

Until now there have been no theoretical or experimental investigations on the spin structure of these systems. In order to shed light onto the existence of such magnetic structures we have performed *ab initio* calculations for Cr and Mn UML on a hexagonal lattice with the Cu lattice constant, simulating Cr and Mn monolayers on Cu(111). Calculations for Cr and Mn UML with the Ag lattice constant, not shown here, lead qualitatively to very similar results. The UML represent a model for monolayers on noble-metal substrates, because the hybridization between a transition-metal overlayer and a noble-metal substrate is small. The investigation included the following different magnetic structures for a comparison of the total energy:

(i) The ferromagnetic p(1×1) structure.

(ii) The row-wise antiferromagnetic structure as shown in figure 4(a). The unit cell of this configuration contains two atoms (cf. figure 4(b)). The ferromagnetic structure and the antiferromagnetic structure are connected by a continuous rotation as indicated in figure 4(b).

(iii) The 120° configuration, which the n.n. Heisenberg model predicts to be energetically preferable for antiferromagnetic materials. The corresponding $(\sqrt{3} \times \sqrt{3})$R30° unit cell is shown in figure 4(d). It is again possible to go from the ferromagnetic structure to the 120° configuration by a continuous rotation, rotating two atoms by the same angle α but in opposite directions, as indicated in figure 4(d). If this rotation is continued up to $\alpha = 180°$, the system arrives at an additional collinear antiferromagnetic structure, which will be denoted as the 180° configuration.

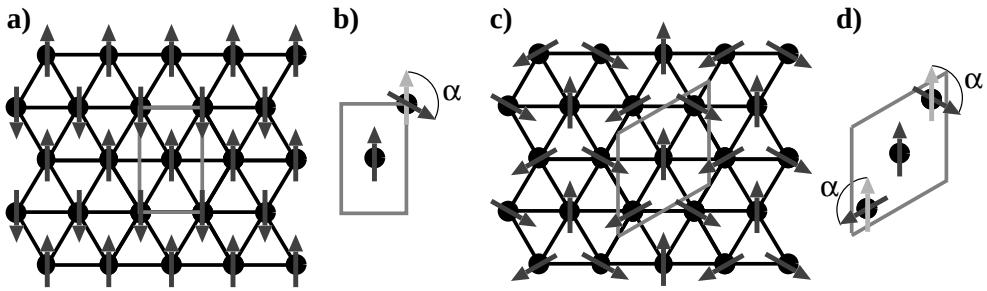

Figure 4. (a) The row-wise antiferromagnetic structure. (c) The non-collinear 120° configuration. The ferromagnetic structure can be transformed by a continuous rotation into structure (a) as indicated in (b) and into structure (c) as indicated in (d).

The results of the calculations are presented in figure 5. The plots show the total energy (circles, left-hand scale) and the magnetic moments (up-pointing and down-pointing triangles, right-hand scale) as functions of the rotation angle α. The left-hand panels show rotations that transform the ferromagnetic structure into the row-wise antiferromagnetic structure. The right-hand panels show the rotations according to figure 4(d). The scales of the left- and right-hand panels are equal; they differ, however, for Cr (upper panels) and Mn (lower panels).

Consider first Cr: starting from the row-wise antiferromagnetic solution (figure 5 upper left-hand panel) and rotating the direction of the magnetic moment towards the ferromagnetic structure, the magnetic moment decreases rapidly and finally disappears at $\alpha \approx 60°$. Thus, a ferromagnetic solution for the Cr(111) UML with the lattice constant of Cu does not exist. Although the moment changes drastically, the energy shows a cosine-like behaviour in the region where a magnetic solution exists, as the n.n. Heisenberg model predicts for an

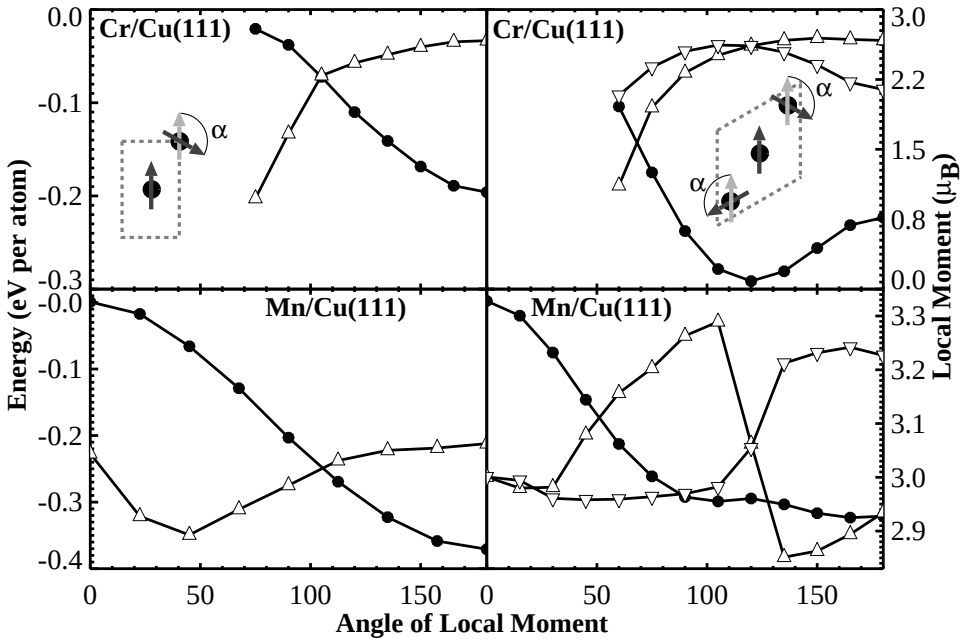

Figure 5. The calculated energy (filled circles) and magnetic moments (filled triangles) as functions of the rotation angle of the local moment for the UML of Cr (upper panels) and that of Mn (lower panels) with the Cu(111) geometry. Generally, the moments of the centre atom (up-pointing triangles) and the outer atoms (down-pointing triangles) differ in the unit cell with three atoms.

antiferromagnet. The total energy along the rotation path in the unit cell in figure 4(d) (figure 5 upper right-hand panel) reveals a pronounced minimum at 120°. This minimum and the shape of the energy curve match very well the expectation from the Heisenberg model, although again the moments vanish at $\alpha \approx 60°$, when the system is rotated towards the ferromagnetic state. It is clearly visible that the 120° configuration is the lowest-energy configuration among all configurations studied here. Thus, it is the magnetic ground state of the Cr UML predicted by the present investigation.

Now turning to Mn and comparing the results for the two-atom unit cell (figure 5 lower left-hand panel) with those for Cr (figure 5 upper left-hand panel) we find that the behaviours of Mn and Cr are very similar, i.e. the energy curve is cosine-like and Mn prefers to be antiferromagnetic. However, in contrast to the case for Cr, the ferromagnetic state exists and the magnetic moments change only within a narrow range, 2.9 μ_B–3.05 μ_B, with the rotation. The lower right-hand panel reveals a surprise: the total energy of the Mn system with three atoms per unit cell does not exhibit a minimum at 120°, as commonly expected from the classical Heisenberg model. In fact, the energy curve is almost flat between 100° and 180°. Apparently, the 180° configuration is even lower in energy than the 120° configuration. This unexpected result cannot be explained within the context of the Heisenberg model as due to higher spin interactions, i.e. the four-spin interaction due to the itinerant nature of the conducting electrons [36]. In summary, the lowest-energy configuration among all magnetic structures investigated is the row-wise antiferromagnetic configuration. We have repeated the Mn calculations including the Cu substrate, using a five-layer slab. The results agree very well with the UML ones. The magnetic enhancement is slightly reduced due to the hybridization with the substrate. The magnetic moment of the ferromagnetic state reduces from 3.04 μ_B

for the UML to 2.89 μ_B on the substrate, and the total-energy difference between the ferromagnetic state and the 180° configuration reduces from 0.25 eV (UML) to 0.24 eV, but the 120° structure remains an energetically unfavourable configuration.

3.2. Magnetic exchange coupling of 3d-metal monolayers on Fe(001)

3d monolayers on Fe(001) face the additional complication that the d–d hybridization of the 3d monolayers with the Fe substrate can lead to 3d metals which couple ferromagnetically or antiferromagnetically to the Fe substrate, and complex spin structures as ground states can be anticipated. In this section we report on a set of systematic investigations of 3d-transition-metal monolayers as overlayers on Fe(001). The calculations are carried out within the GGA using the theoretically determined Fe lattice constant of $a_{\|} = 5.33$ au. Three competing spin structures had been considered: the p(1 × 1) ferromagnetic (FM), the p(1 × 1) layered antiferromagnetic (LAF), and the c(2 × 2) ferrimagnetic (FI) spin configurations (cf. figure 1).

The local magnetic moments of the three spin structures are shown in figure 6(a). We show results from calculations for structurally unrelaxed monolayers—monolayer atoms located at the ideal, pseudomorphic Fe atom sites. The calculations show that for most 3d-metal overlayers (Cr, Mn, Fe, Co) on Fe(001) all three configurations exist and are stable. Only the V monolayer was found to couple exclusively in a layered antiferromagnetic fashion and

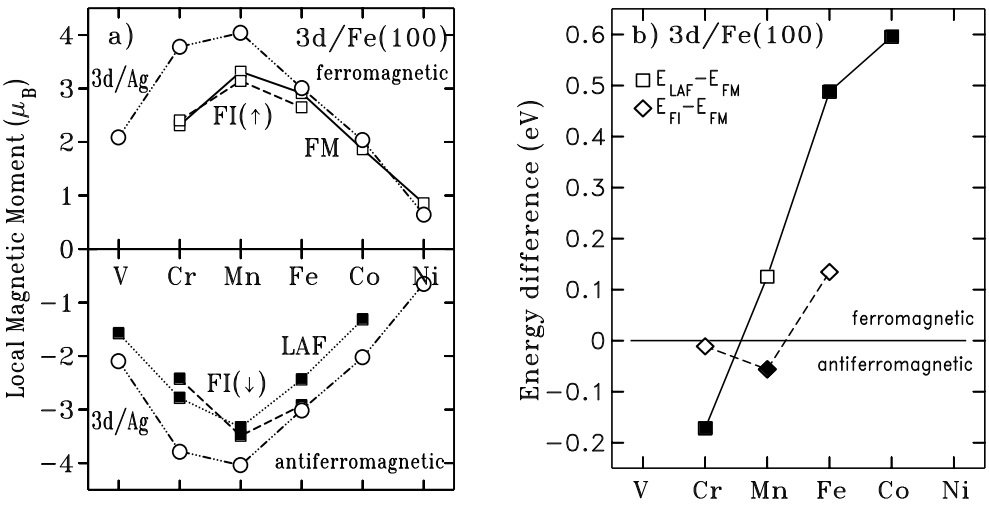

Figure 6. (a) Local magnetic moments of unrelaxed 3d-transition-metal monolayers on Fe(001). A positive (negative) sign of the moments indicates an (anti)ferromagnetic, FM (AF), spin alignment with the Fe substrate, emphasized by open (filled) symbols. We show results for three different spin configurations: p(1 × 1) FM (solid line), p(1 × 1) LAF (dotted line), and the c(2 × 2) FI (dashed lines) for positive and negative moments. The figure is complemented with results for 3d monolayers on Ag(001) (◯ connected by a dash–three-dotted line). As the Ag substrate is non-magnetic, ferromagnetic and antiferromagnetic spin alignments are indistinguishable and moments are identical and are shown twice, once for positive and once for negative sign. (b) The total-energy differences $\Delta E_1 = E_{LAF} - E_{FM}$ between the p(1 × 1) layered antiferromagnetic and the ferromagnetic coupling (squares connected by solid lines) and $\Delta E_2 = E_{FI} - E_{FM}$ between the c(2×2) ferrimagnetic and the p(1×1) ferromagnetic coupling (diamonds connected by dashed lines) of 3d-transition-metal monolayers with Fe(001). The ferromagnetic (layered antiferromagnetic or ferrimagnetic) coupling is energetically preferred for $\Delta E > 0$ (<0). The layered antiferromagnetic coupling is preferred over the ferrimagnetic coupling if $\Delta E_1 < \Delta E_2$. A filled square or diamond indicates the magnetic ground state. For V and Ni only one magnetic state has been found.

the Ni monolayer was found to couple exclusively ferromagnetically to the Fe(001) substrate. Surprisingly, the ferromagnetic moments ($M > 0$), the layered antiferromagnetic moments ($M < 0$), and the two different magnetic moments ($M_1 > 0$ and $M_2 < 0$) for the ferrimagnetic phase are all similar in size. The largest magnetic moment of about 3 μ_B was found for Mn, and then the magnetic moments drop for elements to the left and right of Mn, which is reminiscent of the behaviour on the noble-metal substrates. In order to see the effect of the substrate hybridization on the size of the local moments, the local magnetic moments of 3d-metal monolayers on Ag(001) [37] are included for comparison. Fe ($a_{\|} = 5.33$ au) and Ag ($a_{\|} = 5.51$ au) have very similar in-plane lattice constants and very similar in-plane d–d hybridizations may be expected, but the d–d hybridizations across the interface are very different. From figure 6(a) one infers that the magnetic moments for the Fe, Co, and Ni monolayers are rather independent of the substrate. But increasing deviations are obtained for the monolayer moments in the sequence from Mn to V. The extent of the 3d wavefunction increases for chemical elements from the end of the 3d series to the beginning of the series. Accordingly, the d–d hybridization within the monolayer and between the monolayer and the Fe substrate increases and visibly reduces the magnetic moments for Mn, Cr, and V.

Since the local magnetic moments of the three different magnetic states for Cr, Mn, Fe, and Co monolayers on Fe(001) are very similar in size, total-energy calculations have been performed to determine the minimum-energy magnetic configuration. The energy differences $\Delta E_1 = E_{LAF} - E_{FM}$ between the layered antiferromagnetic and ferromagnetic configuration and $\Delta E_2 = E_{FI} - E_{FM}$ between the c(2 × 2) ferrimagnetic and the ferromagnetic configuration, ignoring again any monolayer relaxation, are shown in figure 6(b). For V and Ni monolayers, which show only one magnetic solution, no data points are included. As has been reported in the literature [42–44], we find, with the exception of in the Cr case, that the ferromagnetic coupling ($\Delta E_1 > 0$) is energetically always more favourable than the layered antiferromagnetic coupling, and that for Cr and Mn the ferrimagnetic coupling ($E_2 < 0$) is energetically preferred over the ferromagnetic coupling. For Fe, Co, and Ni, the ferromagnetic solution is the most stable one. When we compare for Cr or Mn the energies among the three different magnetic phases, we find that for Cr the layered antiferromagnetic coupling is the magnetic ground state, energetically followed by the ferrimagnetic and the ferromagnetic coupling, which are metastable phases. The total-energy differences between FM and LAF configurations and between FM and FI show some differences from those of Handschuh and Blügel [43] coming mostly from the different choice of the in-plane lattice constant. Summarizing, (i) the magnetic ground-state structures are LAF for V and Cr, FI for Mn, FM for Fe, Co, and Ni, and (ii) for the Mn monolayer we find a second spin configuration with an energy about 55 meV/Mn above the ground-state structure.

Therefore, extending the search for the magnetic ground state of Mn to larger surface unit cells may lead to a more complicated ground-state spin structure. Elmouhssine *et al* [45] and Asada *et al* [46] investigated the possibility of additional low-energy spin structures in the p(2 × 2) surface unit cell containing four Mn surface atoms. Two additional spin structures were included: the p(2 × 2) FM magnetic structure with three Mn atoms out of four coupling ferromagnetically to the Fe substrate and one Mn atom coupling antiferromagnetically, as well as the p(2 × 2) AF structure, which is the layered antiferromagnetic version of p(2 × 2) FM, where three Mn atoms couple antiferromagnetically and one atom couples ferromagnetically to Fe. Indeed the calculations reveal that on Fe(001), the Mn c(2 × 2) FI and the p(2 × 2) FM are nearly degenerate ground states. This is obvious from figure 7, which displays the energies of the different configurations relative to the c(2 × 2) FI state energy. Tight-binding linear muffin-tin-orbital calculations by Elmouhssine *et al* found that the p(2 × 2) FM superstructure is 15 meV higher in energy than the c(2 × 2) one, while Asada *et al* found by means of FLAPW calculations

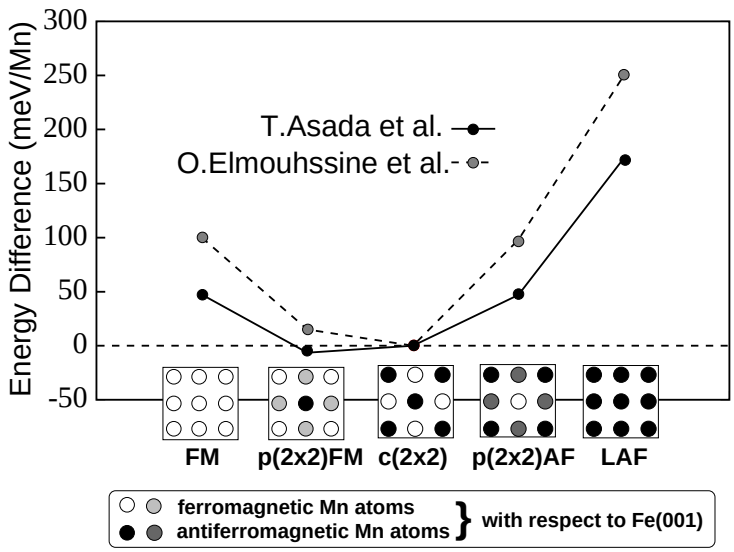

Figure 7. The relative energy $E - E_{c(2\times2)}$ for the five magnetic configurations in units of meV. The small energy difference between the c(2×2) FI state and the p(2×2) FM configuration indicates that the two solutions are nearly degenerate ground states.

that the total energy of the p(2×2) FM superstructure is slightly lower by 6.4 meV/Mn than the c(2×2) FI structure. In any case the energy differences are comparable to the thermal energy at room temperature. Thus atomic relaxations, surface roughness, and thermal excitations in true experimental situations could lead to the coexistence of these two magnetic configurations and thus the appearance of magnetic domains within the Mn monolayer. At present one cannot exclude the possibility of magnetic states with even lower energy not included yet. Further theoretical and experimental investigations are necessary before one can come to a definite conclusion on this matter.

3.3. Comparison to experiment: Cr on Fe(001)

3.3.1. Energetic stability of one monolayer of Cr on Fe(001). Until now, all of the *ab initio* investigations on ultrathin magnetic films on diverse substrates discussed above described the ideal pseudomorphic film with atoms located in the hollow sites formed by the adjacent substrate atoms. These investigations described well the electronic and magnetic properties of pseudomorphically grown films, within one surface terrace of at least 15 atoms across. In general, however, it is experimentally very difficult to achieve pseudomorphic growth conditions. This is particularly true for transition-metal films grown on noble-metal substrates [40], but also for transition-metal films grown on transition-metal substrates. In general, the growth mode of crystals depends on many external parameters as well as materials properties.

In this context Cr/Fe(001) deserves a particular mention. It has developed to a model system for the understanding of the phenomena of exchange coupling between ferromagnetic layers separated by a non-magnetic layer. High-quality Fe/Cr/Fe(001) structures are possible because of the excellent Fe–Cr lattice match and the availability of near-perfect, single-crystal Fe whisker substrates [47]. Under the right growth conditions, structures produced experimentally can closely approximate those presumed in theoretical calculations. However,

a more detailed investigation by Davies *et al* [48] shows that Cr growth under layer-by-layer conditions on Fe(001) leads to the formation of a CrFe alloy, and there is a tendency of Cr atoms to diffuse into the Fe substrate, while Fe atoms are lifted onto the surface, forming islands. Cr exists only as impurities in the Fe(001) surface at low coverage and a disordered surface alloy is formed at higher coverage. The spatial correlation between the Cr atoms was evaluated and it was concluded that on average there are no nearest-neighbour Cr pairs in this alloy at the surface and the surface is of c(2×2) symmetry, where each Cr atom is surrounded by Fe atoms indicating repulsive Cr–Cr pair interactions.

This section is dedicated to shedding some light on the aspect of the stability of the Cr monolayer with respect to the surface-alloy formation and the diffusion into the Fe substrate. We calculated the magnetic moments, the magnetic structures, and the total energies for two types of Cr/Fe(001) system: (i) first, the c(2 × 2) CrFe/Fe(001) substitutional surface alloy (a one-monolayer-thick alloy film of Fe and Cr atoms, with a checkerboard arrangement of Cr and Fe sites, cf. figure 8); and (ii) second, a c(2 × 2) CrFe/Fe(001) substitutional alloy monolayer buried in Fe(001). By comparing the total energies of (i) and (ii) we extract the total-energy difference, ΔE_I, which is interpreted as an interdiffusion energy indicating the stability of the surface alloy against bulk interdiffusion. The formation energy, ΔE_F, of the surface alloy

$$\Delta E_F(\{M\},\{\Delta z_M\}) = E_{\mathrm{c(2\times2)CrFe/Fe(001)}}(\{M\},\{\Delta z_M\}) - \frac{1}{2}\Big(E_{\mathrm{Cr/Fe(001)}}(\{M\},\{\Delta z_M\}) + E_{\mathrm{Fe(001)}}\Big) \quad (1)$$

is determined by the total-energy difference between the system containing the surface alloy, $E_{\mathrm{c(2\times2)CrFe/Fe(001)}}$, and the average of the total energies determined by the Cr monolayers on Fe(001), $E_{\mathrm{Cr/Fe(001)}}$, and the clean Fe(001) surface, $E_{\mathrm{Fe(001)}}$. Although, what occurs in real growth would be strongly governed by the energy barriers of each process, we believe that the examination of such total-energy aspects will give a certain indication of how systems evolve.

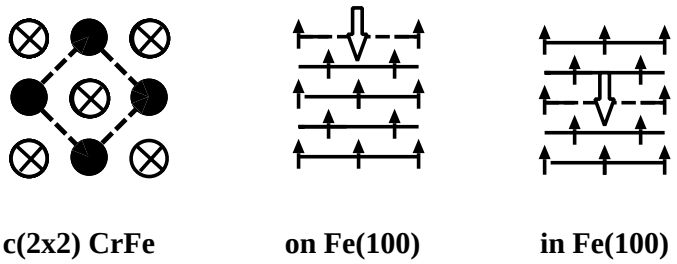

Figure 8. A schematic representation of the top view of the c(2 × 2) surface unit cell of the CrFe surface alloy, and side views of a CrFe alloy sheet on the Fe(001) surface and in the Fe bulk, with Cr atoms antiferromagnetically aligned with Fe.

The formation and the interdiffusion energy depend (i) on the magnetism $\{M\}$: (a) the local moments as well as (b) the magnetic ground-state structure; and (ii) on the atomic structure $\{\Delta z\}$, which depends also on the magnetic structure. The latter is not further discussed here. The magnetism $\{M\}$ enters twice due to two different magnetic structures of the different systems. Thus for each system we investigated first the minimum-energy ground-state magnetic structure and then compared the magnetic energies. The magnetic moment of Cr depends sensitively on the in-plane lattice constant of Fe chosen, the interlayer relaxation, and the choice of the exchange–correlation approximation to the density functional theory.

In order to make our study transparent as regards comparison to earlier investigations on the electronic structure and magnetism of these systems, we present the magnetic structure and magnetic moments for the Cr/Fe system. In all three structural configurations, a Cr monolayer on Fe(001), or the c(2×2) CrFe surface alloy on Fe(001) or buried in the bulk, the lowest energy was found when the Cr atom was aligned antiferromagnetically with Fe. The magnetic moments of Cr are $-1.78\ \mu_B$, $-2.63\ \mu_B$, and $-0.74\ \mu_B$ for the monolayer, surface alloy or alloy buried in bulk, respectively. The negative sign in front of the magnetic moments expresses the antiferromagnetic alignment of the magnetic Cr moment with Fe. The magnetic moment of the Cr atom in the surface alloy is already close to the value of the magnetic moment ($-2.75\ \mu_B$) of a single Cr atom in the Fe(001) surface [49].

We found that the alloy formation is favoured by about 0.4 eV/atom, and an energy of 0.04 eV/atom is gained if Cr diffuses to a deeper layer. The latter energy is rather small and may change upon lattice relaxation. The alloy formation energy is rather large, is consistent with the experimental finding of Davies *et al*, and is very close to the exchange energy of a single Cr atom with an Fe atom at the Fe(001) surface [50].

3.3.2. STS for the c(2×2) CrFe/Fe(001) surface alloy. The results on the atomic-scale observation of the CrFe surface alloy found by Davies *et al* [48] have been obtained on the basis of spectroscopy measurements with the scanning tunnelling microscope (STM) [51]. Although applied with great success in the field of metal surfaces, including providing the possibility of discerning the different chemical species on the surface, the ability of the STM to resolve magnetic structures is yet to be proved and there is currently much activity in this field. In this section we compare experiments performed on the CrFe surface alloy on Fe(001) with first-principles calculations made on the basis of the Tersoff–Hamann model [52,53]. The main point in this successfully applied theory (see e.g. [54, 55]) is the fact that the differential conductivity measured in STS is proportional to the LDOS of the sample at the position of the tip apex atom.

Figure 9 displays the ST spectra of this experiment in comparison with our calculation of the LDOS above the CrFe surface alloy. Far away from any of the impurities, which were clearly visible in the topography mode, the measured spectrum is identical to that of the clean Fe(001) surface, i.e. it shows the known d_{z^2} surface resonance peak [54]. On the other hand, near to an impurity, in islands as well as in the substrate, the spectrum displays two small peaks at about -0.3 V and +0.25 V. Thereby it was concluded that the impurities are Cr while the islands consist of Fe which has been lifted to the surface by processes of exchange with Cr.

To verify these conclusions, we compare the calculated LDOS on top of the Cr atom in the surface alloy with the experimental spectrum of a Cr impurity (see figure 9). One finds two peaks in the LDOS near the Fermi energy located at -0.5 eV and +0.1 eV. The energy difference is thus 0.6 eV which is in excellent agreement with the measured difference of 0.55 V. The shift of about 0.15 eV with respect to the experiment is within the error which has been found for the Fe(001) surface, and is partly ($\Delta E = 0.09$ eV) due to the choice of the lattice constant (the theoretical LDA lattice constant of Fe, $a_0 = 5.23$ au, instead of the experimental lattice constant of $a_0 = 5.41$ au), and partly due to the choice of the LDA to the density functional theory, the approximation of the Cr impurity by a CrFe surface alloy, and, in general, it depends on the size of the Cr magnetic moment [56]. Notice also that the occupied state is a rather broad feature while the unoccupied state is quite sharp. This is also observed in the experiment (see figure 9), and, therefore, we are confident that these states are the origin of the STS peaks.

Since the unoccupied state is close in energy to the original d_{z^2} surface resonance of Fe(001) it was speculated in reference [48] that it is closely related to it. Our calculations

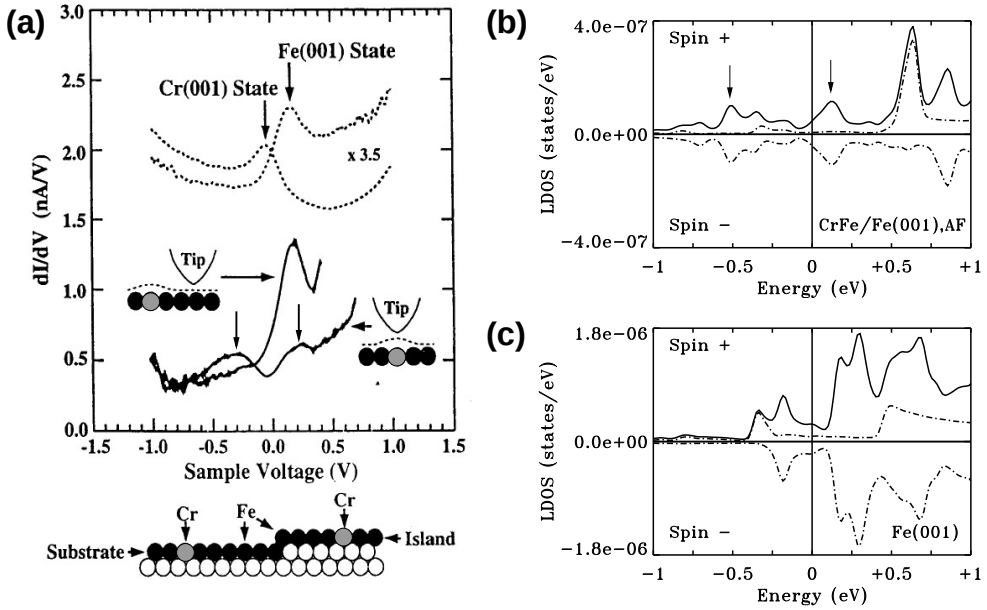

Figure 9. Comparison of the STS experiment on the CrFe/Fe(001) surface alloy [48] (a) with the calculated LDOS of the c(2×2) CrFe/Fe(001) surface alloy (b) and of the clean Fe(001) surface (c). Panel (a) is taken from reference [48] and displays the spectrum of the clean Cr(001) and Fe(001) surfaces as well as the spectrum near a Cr atom of the surface alloy and far away from it. The LDOS (b) and (c) have been calculated for on top of the Cr atom in c(2 × 2) CrFe/Fe(001) and for the Fe atom of the clean Fe(001) surface at distances of $z = 6.7$ Å and $z = 6.5$ Å, respectively. Full lines in (b) and (c) represent the total LDOS while the dot–dashed lines display the majority- and minority-spin contributions. There is an excellent agreement between theory and experiment, although the calculated results are shifted with respect to the experiment by about +0.15 V.

reveal that this state is indeed a strongly localized d_{z^2} surface state although with the origin at the Cr atom and not at the Fe atom. The occupied state, appearing in the ST spectrum, on the other hand, results from a state with a strong hybridization between the Cr and Fe surface atoms. However, for single Cr impurities [56] at the Fe(001) surface, d_{z^2} is not located at the Cr atom and it is instead a d_{z^2} state localized at the Fe site.

3.3.3. Magnetic identification: STS for the Cr ML on Fe(001). In this section we present calculations of the LDOS in the vacuum for the three different magnetic configurations of a Cr monolayer on Fe(001) considered in the previous sections. On one hand, the aim is to investigate possibilities of discerning the magnetic configurations on the basis of STS. On the other hand, we check whether peaks in the LDOS allow chemical sensitivity as has been presumed in the previous part.

We find a highly structured spectrum for the ferromagnetic Cr monolayer with a dominating minority-state peak at about +0.2 eV (figure 10). This state appears at the same energy as the known d_{z^2} surface resonance of pure Fe(001) [54] and also results from minority states with d_{z^2} character at the $\bar{\Gamma}$ point of the 2D Brillouin zone (2BZ). It is therefore impossible to distinguish the ferromagnetic Cr monolayer from the pure Fe(001) surface on the basis of STS (non-spin-polarized as well as spin-polarized), since the other strong features lie quite high in energy and may not be accessible to STS. If we now turn to the layered antiferromagnetic

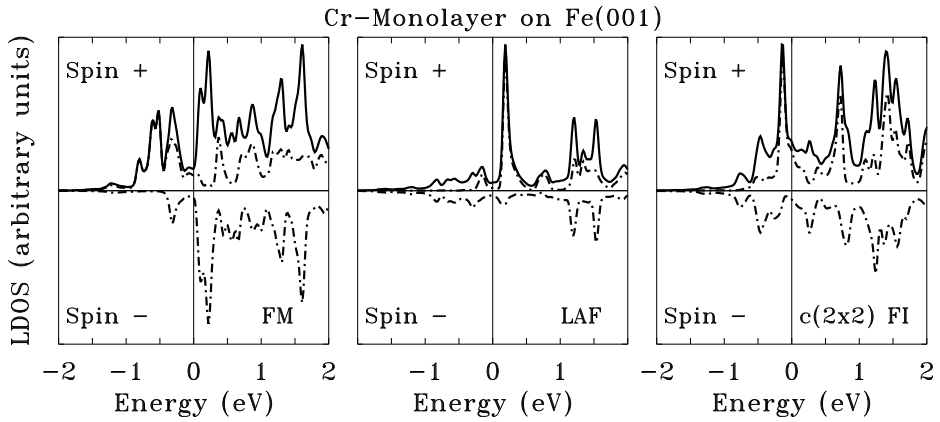

Figure 10. The calculated LDOS of Cr monolayers on Fe(001) for different magnetic configurations: ferromagnetic (FM), layered antiferromagnetic (LAF), and c(2×2) (anti)ferrimagnetic (FI) at a distance of $z_0 = 7$ Å above the surface. The upper part of each panel is for majority states (spin +); the lower part is for minority states (spin −) (dot–dashed lines). The full line represents the total contribution of both spin directions in each case. The Fermi energy is the origin of energy zero.

configuration, which is the ground-state configuration for Cr [43], we again find a feature at a voltage of +0.2 eV, but resulting from majority states and lying in the pseudogap between the Fe majority and the Cr majority states (again located at the $\bar{\Gamma}$ point and of d_{z^2} character). The indistinguishability between the LAF Cr monolayer and the pure Fe(001) surface still holds for this magnetic configuration on the basis of non-spin-polarized STS. However, spin-selective STS should be able to show a difference, since the features originate from majority (Cr) and minority (Fe) states. An important remark has to be made concerning the experiment of Davies *et al* [48] discussed in the previous section. The islands found on the surface after Cr deposition were identified as consisting of Fe atoms on the basis of the ST spectrum displaying a sharp peak at +0.2 V. However, this feature is also found in our calculation for the layered antiferromagnetic Cr monolayer and it should thus be impossible to discern the chemical difference by means of STS. Still, their interpretation of intermixing has been verified by Auger electron spectroscopy [57]. It should be kept in mind though that such interpretations based on STS can be misleading if materials of very similar electronic structure are present and the structural differences are small.

Finally, there are two majority-state peaks for the c(2×2) (anti)ferrimagnetic configuration at −0.15 eV (d_{z^2}) and at +0.7 eV resulting from the ferromagnetically and antiferromagnetically aligned Cr atoms, respectively, as can be deduced by comparing the DOS of the three different spin structures. These two peaks should provide the possibility of distinguishing this magnetic state from the layered antiferromagnetic or ferromagnetic one as well as from the pure Fe(001) surface. Two further remarks are worth making. First, there are two minority-state features appearing at −0.5 eV and +0.2 eV caused by states of the antiferromagnetic Cr atom, which have no significance for the total spectrum since the above-mentioned occupied majority states dominate the spectrum. However, these states dominated for the CrFe surface alloy as has been discussed in the previous section, and their occurrence is only due to the antiferromagnetic coupling of one Cr atom to the Fe substrate. Second, one can find a spin-split partner of the majority state at +0.7 eV coming from the ferromagnetic atom with only slightly higher energy, which therefore does not give an extra peak in the total spectrum.

4. Final remarks

We have presented results of systematic investigations of the magnetism, the magnetic interactions, and the magnetic coupling of magnetic monolayers on non-magnetic and magnetic substrates. Of course, the results are necessarily incomplete as we have not discussed the magnetic anisotropy or the effect of structural relaxations, reconstructions, and structural defects such as steps. First-principles calculations for thick films such as fcc Fe on Cu(001) [11] or very thick films such as for the Fe/Cr/Fe(001) systems [58, 59] have just become possible. New challenges driven by nano-magnetism and magneto-electronics are already in sight.

Acknowledgments

This work was supported by the DFG under Grants BL444/1-1 and WI1277/6-1, the programme 'Verbundforschung Synchrotronstrahlung' of the BMBF, and the TMR Networks, Contract Nos EMRX-CT96-0089 and FMRX-CT98-0178.

References

[1] Bennett L H and Watson R E (ed) 1993 *Magnetic Multilayers* (Singapore: World Scientific)
[2] Bland J A C and Heinrich B (ed) 1994 *Ultrathin Magnetic Structures I, II* (Berlin: Springer)
[3] Zhu M J, Bylander D M and Kleinman L 1991 *Phys. Rev.* B **43** 4007
[4] Eriksson O, Albers R C and Boring A M 1991 *Phys. Rev. Lett.* **66** 1350
[5] Blügel S 1992 *Europhys. Lett.* **18** 257
[6] Wu R and Freeman A J 1992 *Phys. Rev.* B **45** 7222
[7] Blügel S 1992 *Phys. Rev. Lett.* **68** 851
[8] Reddy B V, Khanna S N and Dunlap B I 1993 *Phys. Rev. Lett.* **70** 3323
[9] Cox A J, Louderback J G and Bloomfield L A 1993 *Phys. Rev. Lett.* **71** 923
[10] Tian D, Lin R F, Jona F and Marcus P M 1990 *Solid State Commun.* **74** 1017
[11] Asada T and Blügel S 1997 *Phys. Rev. Lett.* **79** 507 and references therein
[12] Prinz G A 1985 *Phys. Rev. Lett.* **54** 1051
[13] Clarke A, Jennings G, Willis R F, Rous P J and Jennings J B 1987 *Surf. Sci.* **187** 327
[14] Weber W, Kerkmann D, Pescia D, Wesner D A and Güntherodt G 1990 *Phys. Rev. Lett.* **65** 2058
[15] Freeman A J and Wu R 1991 *J. Magn. Magn. Mater.* **100** 497
[16] Weinert M and Blügel S 1993 *Magnetic Multilayers* ed L H Bennett and R E Watson (Singapore: World Scientific)
[17] Flores T, Hansen M and Wuttig M 1992 *Surf. Sci.* **279** 251
[18] Gunnarsson O 1976 *J. Phys. F: Met. Phys.* **6** 587
[19] Janak J F 1977 *Phys. Rev.* B **16** 255
[20] Grünberg P, Schreiber R, Pang Y, Brodsky M B and Sowers H 1986 *Phys. Rev. Lett.* **57** 2442
[21] Parkin S S P, More N and Roche K P 1990 *Phys. Rev. Lett.* **64** 2304
[22] Baibich M N, Broto J M, Fert A, Nguyen Van Dau F, Petroff F, Etienne P, Creuzet G, Friederich A and Chazelas J 1988 *Phys. Rev. Lett.* **61** 2472
[23] Binasch G, Grünberg P, Saurenbach F and Zinn W 1989 *Phys. Rev.* B **39** 4828
[24] Dieny B, Speriosu V S, Parkin S S P, Gurney B A, Wilhoit D R and Mauri D 1991 *Phys. Rev.* B **43** 1297
[25] Unguris J, Celotta R J and Pierce D T 1991 *Phys. Rev. Lett.* **67** 140
[26] Grünberg P, Demokritov S, Fuss A, Schreiber R, Wolf J A and Purcell S T 1992 *J. Magn. Magn. Mater.* **104** 1734
[27] Walker T G and Hopster H 1994 *Phys. Rev.* B **72** 1557
Harp G R, Parkin S S P, O'Brien W L and Tonner B P 1995 *Phys. Rev.* B **51** 3293
Fuchs P, Totland K and Landolt M 1996 *Phys. Rev.* B **53** 9123
Ciccacci F, De Rossi S, Isella G and Magnoni A 1997 *Solid State Commun.* **101** 893
Bencok P, Andrieu S, Arcade P, Richter C, Ilakovac V, Heckmann O, Vesely M and Hricovini K 1998 *Surf. Sci.* **402–404** 327
Huttel Y, Avila J, Asensio M C, Bencok P, Richter C, Ilakovac V, Heckmann O and Hricovini K 1998 *Surf. Sci.* **402–404** 609

[28] Carbone C and Alvarado S F 1987 *Phys. Rev.* B **36** 2433
Hillebrecht F U, Roth Ch, Jungblut R, Kisker E and Bringer A 1992 *Europhys. Lett.* **19** 711
Walker T G, Pang A W, Hopster H and Alvarado S F 1992 *Phys. Rev. Lett.* **69** 1121
Idzerda Y U, Tjeng L H, Lin H-J, Gutierrez C J, Meigs G and Chen C T 1993 *Phys. Rev.* B **48** 4144
Turtur C and Bayreuther G 1994 *Phys. Rev. Lett.* **72** 1557
Stoeffler D and Gautier F 1995 *J. Magn. Magn. Mater.* **147** 260
Venus D and Heinrich B 1996 *Phys. Rev.* B **53** 1733
Pfandzelter R, Igel T and Winter H 1997 *Surf. Sci.* **377–379** 963
[29] Purcell S T, Johnson M T, McGee N W E, Coehoorn R and Hoving W 1992 *Phys. Rev.* B **45** 13 064
Walker T G and Hopster H 1993 *Phys. Rev.* B **48** 3563
Roth Ch, Kleeman Th, Hillebrecht F U and Kisker E 1995 *Phys. Rev.* B **52** 15 691
Rader O, Gudat W, Schmitz D, Carbone C and Eberhardt W 1997 *Phys. Rev.* B **56** 5053
Dresselhaus J, Spanke D, Hillebrecht F U, Kisker E, van der Laan G, Goedkoop J B and Brookes N B 1997 *Phys. Rev.* B **56** 5461
Igel T, Pfandzelter R and Winter H 1998 *Phys. Rev.* B **58** 2430
[30] Vogel J, Panaccione G and Sacchi M 1994 *Phys. Rev.* B **50** 7157
Liberati M, Panaccione G, Sirotti F, Prieto P and Rossi G 1999 *Phys. Rev.* B **59** 4201
[31] Wang Z Q, Li Y S, Jona F and Marcus P M 1987 *Solid State Commun.* **61** 623
Pain P and Eymery J P 1994 *J. Magn. Magn. Mater.* **133** 493
Mijiritskii A V, Smulders P J M , Chumanov V Ya, Rogojanu O C, James M A and Boerma D O 1998 *Phys. Rev.* B **58** 8960
[32] Wimmer E, Krakauer H, Weinert M and Freeman A J 1981 *Phys. Rev.* B **24** 864
Weinert M, Wimmer E and Freeman A J 1982 *Phys. Rev.* B **26** 4571
[33] von Barth U and Hedin L 1972 *J. Phys. C: Solid State Phys.* **5** 1629
[34] Moruzzi V L, Janak J F and Williams A R 1978 *Calculated Electronic Properties of Metals* (New York: Pergamon)
[35] Perdew J P, Chevary J A, Vosko S H, Jackson K A, Pederson M R, Singh D J and Fiolhais C 1992 *Phys. Rev.* B **46** 6671
[36] Kurz Ph, Hirai K and Blügel S 1999 to be published
[37] Blügel S and Dederichs P H 1989 *Europhys. Lett.* **9** 597
[38] Blügel S 1988 *Europhys. Lett.* **7** 743
[39] Újfalussy B, Szunyogh L and Weinberger P 1995 *Phys. Rev.* B **51** 12 836
[40] Blügel S 1996 *Appl. Phys.* A **63** 595
[41] Freeman A J and Fu C L 1987 *J. Appl. Phys.* **61** 3356
[42] Mirbt S, Eriksson O, Johansson B and Skriver H L 1995 *Phys. Rev.* B **52** 15 070
[43] Handschuh S and Blügel S 1998 *Solid State Commun.* **105** 633
[44] Wu R and Freeman A J 1995 *Phys. Rev.* B **51** 17 131
[45] Elmouhssine O, Moraïtis G, Demangeat C and Parlebas J C 1997 *Phys. Rev.* B **55** R7410
[46] Asada T, Bihlmayer G and Blügel S 1999 to be published
[47] Arrott A S, Heinrich B and Purcell S T 1990 *Kinetics of Ordering and Growth at Surfaces* ed M G Lagally (New York: Plenum) p 321
[48] Davies A, Stroscio J A, Pierce D T and Celotta R J 1996 *Phys. Rev. Lett.* **76** 4175
[49] Nonas B, Wildberger K, Zeller R and Dederichs P H 1997 *J. Magn. Magn. Mater.* **165** 137
[50] Nonas B, Wildberger K, Zeller R and Dederichs P H 1998 *Phys. Rev. Lett.* **80** 4574
[51] Binnig G and Rohrer H 1982 *Helv. Phys. Acta* **55** 726
[52] Tersoff J and Hamann D R 1983 *Phys. Rev. Lett.* **50** 1998
[53] Heinze S, Blügel S, Pascal R, Bode M and Wiesendanger R 1998 *Phys. Rev.* B **58** 16 432
[54] Stroscio J A, Pierce D T, Davies A, Celotta R J and Weinert M 1995 *Phys. Rev. Lett.* **75** 2960
[55] Biedermann A, Genser O, Hebenstreit W, Schmid M, Redinger J, Podloucky R and Varga P 1996 *Phys. Rev. Lett.* **76** 4179
[56] Papanikolaou N, Nonas B, Heinze S, Blügel S, Zeller R and Dederichs P H 1999 *Phys. Rev.* B to be submitted
[57] Pfandzelter R, Igel T and Winter H 1996 *Phys. Rev.* B **54** 4496
[58] Hirai K 1999 *Phys. Rev.* B **59** R6612
[59] Niklasson, A M N, Johansson B and Nordström L 1999 *Phys. Rev. Lett.* **82** 4544